Journal of Alloys and Compounds 501 (2010) 339–344

Contents lists available at ScienceDirect

Journal of Alloys and Compounds

journal homepage: www.elsevier.com/locate/jallcom

Comparative effects of indium/ytterbium doping on, mechanical and gas-sensitivity-related morphological, properties of sprayed ZnO compounds

A. Boukhachem[a], S. Fridjine[a], A. Amlouk[a], K. Boubaker[a,*], M. Bouhafs[b], M. Amlouk[a]

[a] Unité de physique des dispositifs à semi-conducteurs, Faculté des sciences de Tunis, Université de Tunis El Manar, 2092 Tunis, Tunisia
[b] Unité de Recherche MA2I, École Nationale d'Ingénieurs de Tunis B.P. 37, Le Belvédère, 1002 Tunis, Tunisia

ARTICLE INFO

Article history:
Received 15 January 2010
Received in revised form 7 April 2010
Accepted 14 April 2010
Available online 24 April 2010

PACS:
2008: 77.84.Bw
81.15.Rs
81.40.Ef
84.60.Jt

Keywords:
Zinc oxide
Opto-thermal expansivity ψ_{AB}
Surface roughness
Indium doping
Optical properties
BPES
Ytterbium doping

ABSTRACT

In this study, conducting and transparent indium-doped zinc oxide (ZnO) thin films have been deposited on glass substrates by the micro-spray technique. First, zinc oxide layers were obtained by spaying a solution of propanol and zinc acetate in acidified medium. Alternatively, some of the obtained films were doped with indium (In) at the molar rates of: 1%, 2% and 3%. In addition to the classical structural investigated using XRD, AFM and SEM techniques, microhardness Vickers (Hv) measurements have been carried out along with comparative morphological prospecting.

The specific gases sensitivity-related surface morphology of the doped ZnO compounds was favorably different from that of the non-doped ones, and showed a thin overlay structure. Results were compared to those recorded for similar ytterbium-doped material.

1. Introduction

Zinc oxide (ZnO) is a hexagonal würtzite structured semiconductor with high piezoelectric and gas-detecting properties [1–7]. Its deposition on polymer substrates has been widely discussed and exploited in the last four decades literature [6–11]. Recently, it has been established that polymers, although having merits of being cheaper and lighter than glass-similar materials, present a higher thermal diffusivity and besides all a weaker mechanical strength. Consequently, glass has been preferred as substrate in the major part of recent applications.

On another hand, the structure and the mechanical performance of the active ZnO layer could not be improved accordingly. Many attempts have been made in this context.

In a lastly carried out investigation [12], an accidental ytterbium doping suggested new routes for hardening such binary structures. This trend was motivated by a recent orientation toward a meaningful contribution of the active layers to the mechanical resistance of the whole sensing devices which are more and more subjected to external solicitations and constraints.

In recent studies, many doping elements for ZnO have been experimented [13–16]. In some studies, the merits of indium as an effective doping agent have been pointed out. Nevertheless, there is a lack of information about the way indium affects ZnO compounds roughness and crystal parameters physical parameters.

In this work, explanations to the paradoxical effects of indium doping at macro and micro levels are presented. Doping techniques and processes have been detailed along with common characterizing means. The last part of this paper is dedicated to the nano-scale analyses and discussions.

2. Experimental details

2.1. Indium-free and indium-doped ZnO films preparation

Indium-free ZnO thin films have been first prepared in a glass substrate temperature domain of 400–500 °C with a mean value of 460 ± 5 °C [17], using propanol and zinc Acetate ($Zn(CH_3CO_2)_2$):10^{-2} M according to the chemical protocol summarized in Fig. 1. Indeed, ethanol and water were used previously [12,17] but the iso-propyl alcohol has been tested as the best to dissolve the zinc acetate and to gives acceptable adherence of ZnO thin films on glass substrate.

* Corresponding author.
E-mail address: mmbb11112000@yahoo.fr (K. Boubaker).

0925-8388/$ – see front matter © 2010 Elsevier B.V. All rights reserved.
doi:10.1016/j.jallcom.2010.04.100

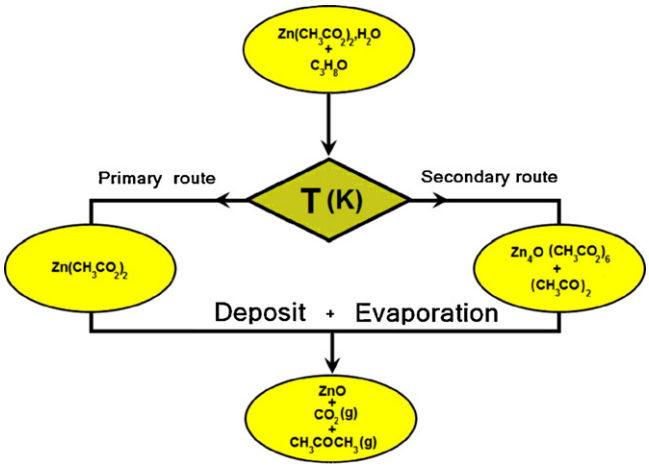

Fig. 1. Zno layers elaboration chemical protocol.

In the beginning of the process, dissolution process involves a simple liquid–liquid dissolution along with a chemical reaction yielding both $Zn_4O(CH_3CO_2)_6$ and CH_3CO. At an intermediary stage, the three compounds ($Zn_4O(CH_3CO_2)_6$, ($Zn(CH_3CO_2)_2$) and CH_3CO) yield evaporated gases and a remaining layered compound (ZnO).

The precursor mixture was acidified using acetic acid (pH 5), the obtained ZnO thin films' thickness was approximately 0.5 μm. These films are designated, in the following parts of the study, as (A) or In-free samples.

Nitrogen was used as the carrier gas (pressure at 0.35 bar) through a 0.5 mm-diameter nozzle. The nozzle-to-substrate plane distance was fixed at the optimal value of 27 cm as demonstrated by Boubaker et al. [18]. During deposition, precursor mixture flow rate was held constant at 4 mL/min.

Indium-doped ZnO:In thin films solution have been fabricated under the same experimental conditions, by adding indium chloride ($InCl_3$, xH_2O, 99.9% purity) to the precursor solution while maintaining acidity level. In the three elaborated samples, the indium-to-zinc molar ratio: In^{3+}/Zn^{2+} was 1, 2 and 3%. The corresponding samples were designated as (B), (C) and (D), respectively.

2.2. Common characterization techniques

Samples (A), (B), (C) and (D) 3D surface topography was examined by atomic force microscopy (AFM) using a VEECO digital instrument 3A microscope in contact mode. Then, the samples films were investigated using X-ray diffractometry by means of a Philips (PW1429) system. The optical transmittance $T(\lambda)$ and reflectance $R(\lambda)$ of the films were recorded using a Schimadzu UV 3100 double-beam spectrophotometer, within a (300–1800 nm) wavelength range.

Finally, a thorough mechanical characterization was carried out using a diamond-pyramidal-indenter Vickers test disposal which is deeply detailed in precedent studies [19,20].

3. Characterization

3.1. Atomic force microscopy (AFM) microanalysis

Fig. 2 shows the 3D AFM micrographs of ZnO (In-free) and indium-doped sprayed layers.

It can be seen that AFM observation concerning In-free sample (A) depicts a disturbed surface with randomly oriented crystallites and a rough surface morphology. On the contrary, the doping has effective role in the enhancement of the crystallinity, Fig. 2. This result is more obvious in AFM surface observations of films prepared at a highly doping (3%). In fact, this doping leads to an improvement of roughness of the ZnO film in which the crystallites are coalescing to form relatively smooth surfaces.

In order to confirm these observations, grains size and roughness measurements have been extracted from AFM data. While the average diameter of the nanograins was 165 nm for the four samples, the mean roughness was noticeably different (Fig. 3). The highly doped ZnO:In films monitor relatively smoother surfaces.

3.2. X-rays diffraction (XRD) analysis

XRD patterns of the deposited ZnO (In-free) along with In-doped films are shown in Fig. 4.

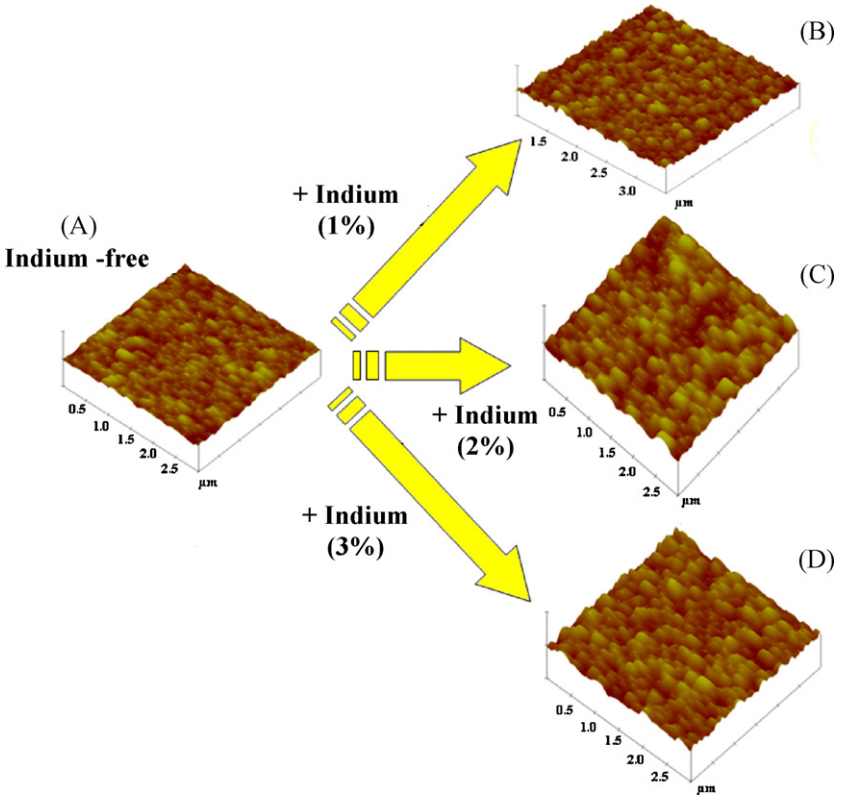

Fig. 2. As-grown layers 3D surface topography.

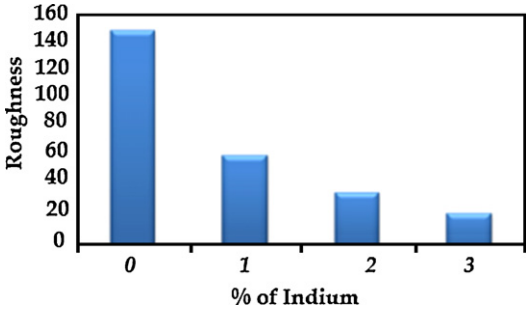

Fig. 3. Indium-doped and indium-free ZnO thin layers roughness (systematic error of ±3%, provided by disposal supplier).

Diagram analysis (Fig. 4) shows that the doped layers (B–D) develop an enhanced preferred orientation of the crystallites with respect to the (0 0 2) reflection oppositely to the In-free films. In general, ZnO layers are identified by XRD peaks: (1 0 1) (1 0 0) and (0 0 2) in hexagonal würtzite system (JCPDS card file no.: 361451 (a = 3.24982, c = 5.20661 Å)). Differently, the doped films c-axis oriented (0 0 2) peaks perpendicular to the glass substrate plane show a very high intensity relatively to other orientations. This feature is associated, as stated by Lucio-Lopez et al. [21], Ratheesh Kumar et al. [22] and Paraguay et al. [23], with a loss of roughness and the appearance of regularly spaced pores resulting in high gas-sensing performances.

3.3. Optical properties

3.3.1. Reflectance and transmission spectra

Figs. 5 and 6 present respectively the reflectance and transmission spectra of the In-free and doped samples.

For the four elaborated samples (A–D), it could be noticed that the transmission coefficient was increasing with doping (from 40% to 85%) while the reflectance remained inside a narrow interval

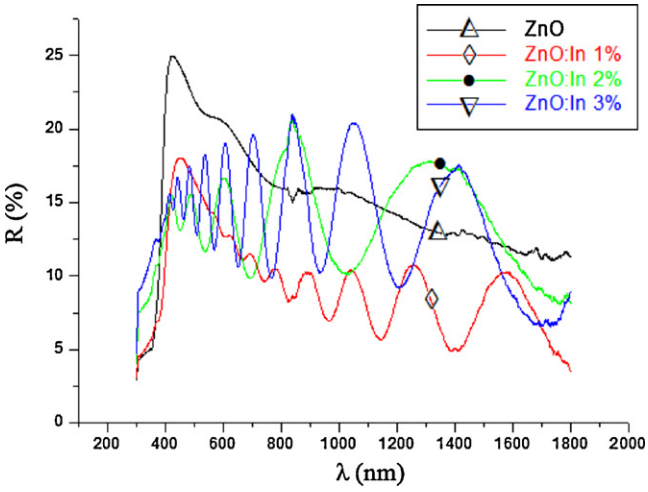

Fig. 5. Reflexion spectra.

(5–20%). These observations confirm the AFM and XRD related consequences of doping on crystal c-axis alignment, which are favorable to light transmission.

4. Comparison with ytterbium doping patterns

4.1. Comparison in terms of Amlouk–Boubaker opto-thermal expansivity ψ_{AB}

The Amlouk–Boubaker opto-thermal expansivity ψ_{AB} is a synthetic physical parameter which has been defined and used in precedent studies [24–39]. This parameter has been defined by:

$$\psi_{AB} = \frac{D}{\hat{\alpha}} \quad (1)$$

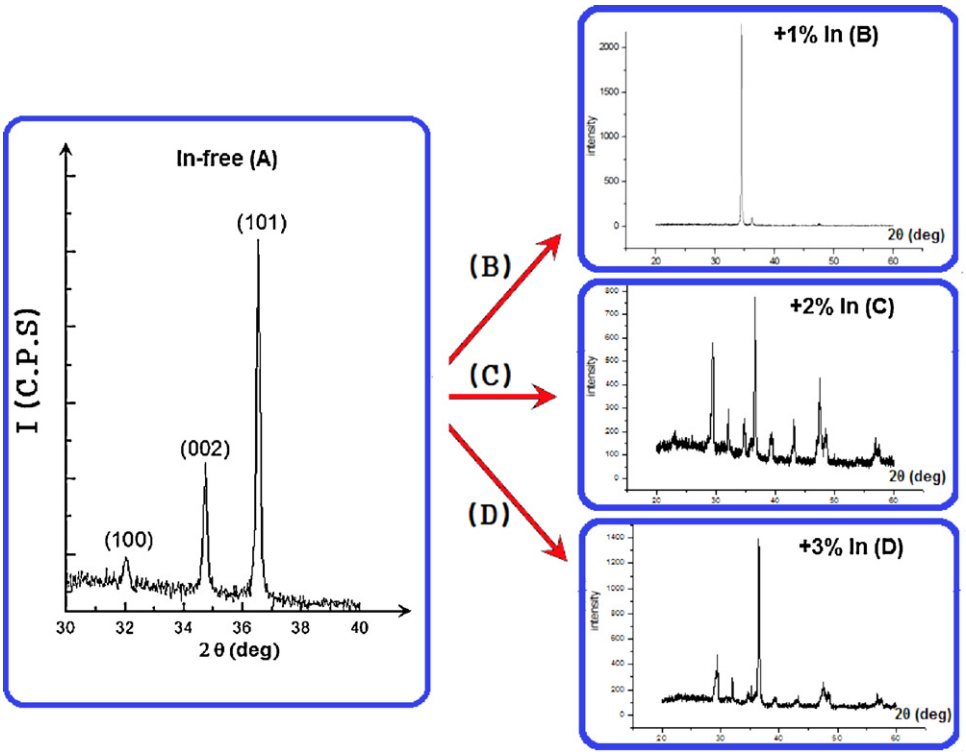

Fig. 4. XRD Diagrams: (A) ZnO, (B) ZnO:In 1%, (C) ZnO:In 2%, (D) ZnO:In 3%.

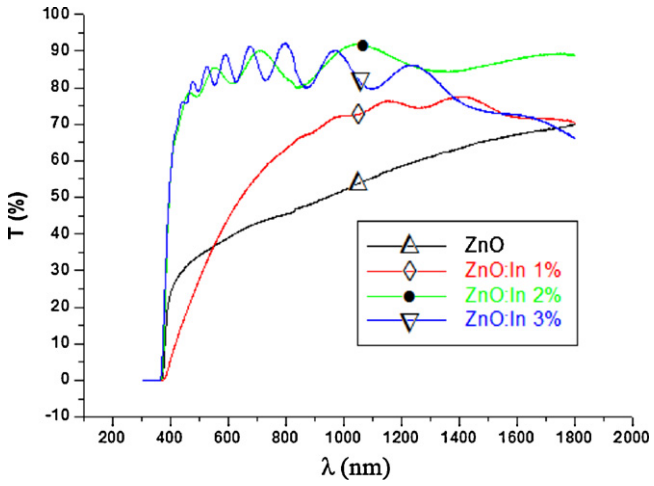

Fig. 6. Transmission spectra.

Table 1
Values of the Amlouk–Boubaker opto-thermal expansivity.

Sample		ψ_{AB} ($m^3\ s^{-1}$)
Yb-doped ZnO	0 ppm	18.2×10^{-12}
	100 ppm	14.5×10^{-12}
	200 ppm	12.9×10^{-12}
	300 ppm	10.1×10^{-12}
In-doped ZnO	0%	18.2×10^{-12}
	1%	9.21×10^{-12}
	2%	8.24×10^{-12}
	3%	11.2×10^{-12}

where D is the thermal diffusivity and $\hat{\alpha}$ is the effective absorptivity.

The effective absorptivity $\hat{\alpha}$, is defined [30–33] as the mean normalized absorbance weighted by $I(\tilde{\lambda})_{AM1.5}$, the solar standard irradiance, with $\tilde{\lambda}$: the normalized wavelength:

$$\hat{\alpha} = \frac{\int_0^1 I(\tilde{\lambda})_{AM1.5} \times \alpha(\tilde{\lambda}) d\tilde{\lambda}}{\int_0^1 I(\tilde{\lambda})_{AM1.5} d\tilde{\lambda}} \quad (2)$$

and where: $I(\tilde{\lambda})_{AM1.5}$ is the reference solar spectral irradiance, fitted using the Boubaker polynomials expansion scheme, BPES.

4.1.1. Determination of the effective absorptivity $\hat{\alpha}$ using the BPES

The normalized absorbance spectrum $\alpha(\tilde{\lambda})$ is deduced from the BPES. According to this protocol: a set of m experimental measured values of the transmittance-reflectance vector $\left(T_i(\tilde{\lambda}_i); R_i(\tilde{\lambda}_i)\right)\big|_{i=1,\ldots,m}$ versus the normalized wavelength $\tilde{\lambda}_i\big|_{i=1,\ldots,m}$ is established. Then the system (3) is set:

$$\begin{cases} R(\tilde{\lambda}) = \left[\dfrac{1}{2N_0}\displaystyle\sum_{n=1}^{N_0} \xi_n \times B_{4n}(\tilde{\lambda} \times \beta_n)\right] \\ T(\tilde{\lambda}) = \left[\dfrac{1}{2N_0}\displaystyle\sum_{n=1}^{N_0} \xi_n' \times B_{4n}(\tilde{\lambda} \times \beta_n)\right] \\ \alpha(\tilde{\lambda}) = \dfrac{1}{d\sqrt{2}}\sqrt{\left(\ln\dfrac{1-R(\tilde{\lambda})}{T(\tilde{\lambda})}\right)^2 + \left(\ln\dfrac{\left(1-R(\tilde{\lambda})\right)^2}{T(\tilde{\lambda})}\right)^2} \end{cases} \quad (3)$$

where β_n are the $4n$-Boubaker polynomials B_{4n} minimal positive roots [30], N_0 is a given integer, d is the layer thickness and ξ_n and ξ_n' are coefficients determined through BPES.

The effective absorptivity $\hat{\alpha}$ is then calculated using Eq. (2).

4.1.2. Determination of Amlouk–Boubaker opto-thermal expansivity ψ_{AB}

The calculated values of the Amlouk–Boubaker opto-thermal expansivity ψ_{AB}, for the ytterbium and indium-doped layers are gathered in Table 1.

This result is in agreement with those of XRD and AFM described above. The increasing c-axis oriented (0 0 2) alignment of ZnO crystallites seems to have positive effects on opto-thermal properties of these doped films via a decrease of ψ_{AB}.

4.2. Comparison in terms of mechanical microhardness

As a guide to performance under variable environmental conditions, the mechanical microhardness has recently attracted designer's attention. The mechanical microhardness of the ytterbium and indium doped layers, has been evaluated in terms of Vickers Hardness (Hv). The characterization test has been carried out using a common diamond-pyramidal-indenter Vickers test disposal whose main parameters are detailed in precedent studies [19,28]. The obtained values are gathered in Fig. 7.

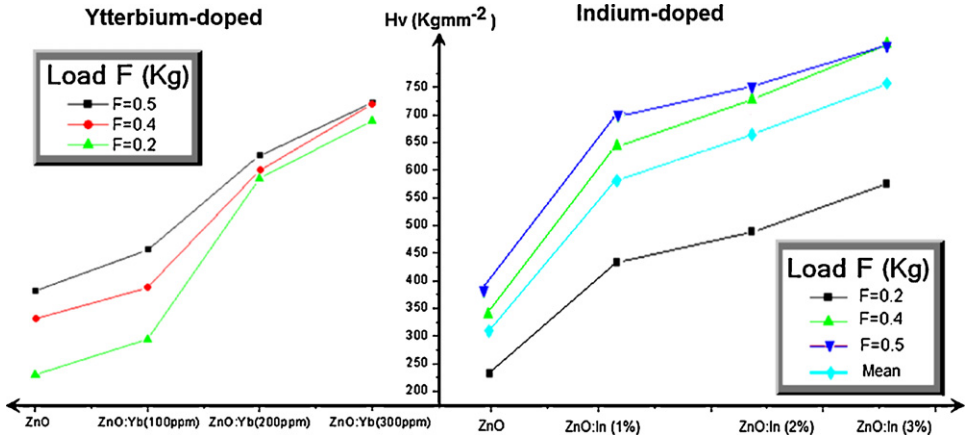

Fig. 7. Vickers Hardness of the doped films.

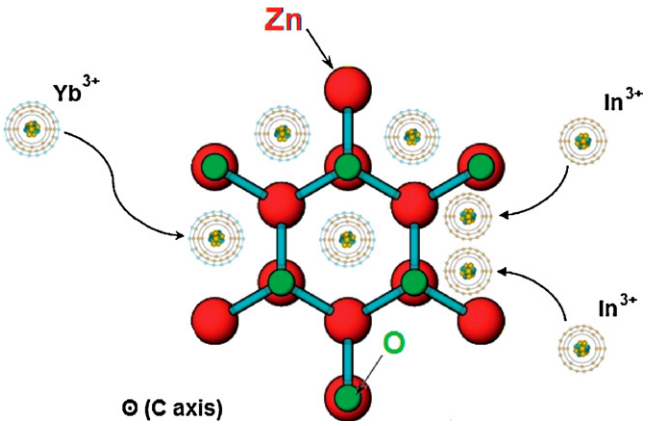

Fig. 8. Doping ions intercalation inside ZnO würtzite matrices.

Fig. 7 summarizes the variation of Hv microhardness with both ytterbium and indium doping. The graphics depicts a conjoint increasing hardness which increases with doping. The main difference lies in the relative amounts of the doping agent.

4.3. Discussion and analysis

As the oxygen-related chemical kinetics and attraction of the two elements Yb and In results in the formation of iso-valent ions: (Yb^{3+} and In^{3+}), explanations of the hardness differences can be set in terms of ionic sizes considerations. In fact, the difference of ionic radii between the two ions is meaningful (Fig. 8). Consequently, it can be suggested that the claimed [40–49] invariance of the ZnO hexagonal matrices, allows exclusively intercalation of smaller ions (i.e., In^{3+}) by, either simple ionic or van der Waals bonding [44–48].

Furthermore, it has been demonstrated elsewhere [12] that the induced decrease of roughness (Fig. 3) results unavoidably in an obvious increase of the resistance to indentation, which is traduced in a high Vickers hardness level. In a recent study of similar compounds, B. Wang *et al.* [50] confirmed that "*the crystals grow in plate-like form in the presence of* In^{3+}". In the same context, Tiburcio-Silver et al. [51] excluded the existence of any indium chemically introduced compound. It means that indium ion In^{3+} has been incorporated inside ZnO würtzute unaltered existing matrices. This presumption has been already formulated when ytterbium ions Yb^{3+} were introduced in the same matrices [12]. If this phenomenon is established and confirmed, it could be a consolidation to the recorded similarities between indium and ytterbium doping under very different relative amounts (some ppm–wt for Yb and 1–3% concentration for In). It was noticed that the two ions In^{3+} and Yb^{3+} have same valences and perform close oxygen-related electronegativities, but have different ionic radii (Fig. 8).

In the same context, Pál and Dékány [52] noticed, while investigating the effect of indium doping on the specific surface and the porosity by subjecting samples to low temperature nitrogen adsorption measurements, that there was no adsorption hysteresis in both pure and lowly indium-doped ZnO [53–56]. They concluded that these samples were not porous. However, the presence of pores was monitored with increasing indium concentration [57]. This feature is in good agreement with the actual XRD, AFM and microhardness analyses.

5. Conclusions

Zinc oxide compounds have been prepared using a low cost spray pyrolysis process. During elaboration and characterization phases, it has been noticed, while doping with indium, that in absence of any conventionally verified chemical reaction of In^{3+} ions, the würtzite structure of ZnO crystals was unchanged. The introduced ions acted apparently only on crystals growth disposition. Comparison with another doping agent (ytterbium) on the basis of roughness and microhardness performance led to interesting conclusions. The intriguing problem of similarity of mechanical behaviours for different doping ions has been discussed in reference to atomistic, stoichiometric and nano-scale considerations. Further studies are actually in progress in order to confirm the suspected effects on gas-sensing performance of similar compounds.

References

[1] P.C. Liao, A. Korotcov, C.W. Huang, Y.S. Huang, D.S. Tsai, K.K. Tiong, J. Alloys Compd. 442 (2007) 313.
[2] L.H. Van, M.H. Hong, J. Ding, J. Alloys Compd. 449 (2008) 207.
[3] W. Lin, J. Pak, D.C. Ingram, A.R. Smith, J. Alloys Compd. 463 (2008) 257.
[4] D.Y. Wang, J. Zhou, G.Z. Liu, J. Alloys Compd. 481 (2009) 802.
[5] D. Beena, K.J. Lethy, R. Vinodkumar, A.P. Detty, V.P. Mahadevan Pillai, V. Ganesan, J. Alloys Compd. 489 (2010) 215–223.
[6] D. Beena, K.J. Lethy, R. Vinodkumar, A.P. Detty, V.P. Mahadevan Pillai, V. Ganesan, J. Alloys Compd. 489 (2010) 215.
[7] I. Saita, T. Toshima, S. Tanda, T. Akiyama, J. Alloys Compd. 446–447 (2007) 80.
[8] Y.M. Kim, M. Yoon, I.W. Park, Y.J. Park, J.H. Lyou, Solid State Commun. 129 (2004) 175.
[9] S.K. Hong, H.Y. Koo, D.S. Jung, I.S. Suh, Y.C. Kang, J. Alloys Compd. 437 (2008) 215.
[10] G. Hu, X. Deng, Z. Peng, Y. Cao, K. Du, J. Alloys Compd. 452 (2008) 462.
[11] P.M. Devshette, N.G. Deshpande, G.K. Bichile, J. Alloys Compd. 463 (2008) 576.
[12] A. Amlouk, K. Boubaker, M. Amlouk, M. Bouhafs, J. Alloys Compd. 485 (2009) 887.
[13] M. Joseph, H. Tabata, T. Kawai, Jpn. J. Appl. Phys. 38 (1999) L1205.
[14] C.S. Hsi, B. Houng, B.Y. Hou, G.J. Chen, S.L. Fu, J. Alloys Compd. 464 (2008) 89.
[15] E. Bacaksiz, M. Parlak, M. Tomakin, A. Özçelik, M. Karakız, M. Altunbaş, J. Alloys Compd. 466 (2008) 447.
[16] K.-S. Kim, H.W. Kim, C.M. Lee, Mater. Sci. Eng. B 98 (2003) 135.
[17] A. Amlouk, K. Boubaker, M. Amlouk, J. Alloys Compd. 482 (2009) 164–167.
[18] K. Boubaker, A. Chaouachi, M. Amlouk, H. Bouzouita, Eur. Phys. J. Appl. Phys. 37 (2007) 105.
[19] T. Ghrib, K. Boubaker, M. Bouhafs, Mod. Phys. Lett. B 22 (2008) 2893.
[20] S. Slama, J. Bessrour, K. Boubaker, M. Bouhafs, Eur. Phys. J. Appl. Phys. 44 (2008) 317.
[21] M.A. Lucio-Lopez, M.A. Luna-Arias, A. Maldonado, M. de la, L. Olvera, D.R. Acosta, Solar Energy Mater. Solar Cells 90 (2006) 733.
[22] P.M. Ratheesh Kumar, S. Kartha, K.P. Vijayakumar, J. Appl. Phys. 98 (2005) 023509.
[23] F. Paraguay, D.J. Morales, W. Estrada, L.E. Andrade, M. Miki-Yoshida, Thin Solid Films 366 (2000) 16.
[24] S. Tabatabaei, T. Zhao, O. Awojoyogbe, F. Moses, Heat Mass Transf. 45 (2009) 1247.
[25] S. Fridjine, M. Amlouk, Mod. Phys. Lett. B 23 (2009) 2179.
[26] O.D. Oyodum, O.B. Awojoyogbe, M. Dada, J. Magnuson, Eur. Phys. J. Appl. Phys. 46 (2009) 21201.
[27] A. Belhadj, O. Onyango, N. Rozibaeva, J. Thermophys. Heat Transf. 23 (2009) 639.
[28] A. Belhadj, J. Bessrour, M. Bouhafs, L. Barrallier, J. Therm. Calorim. 97 (2009) 911.
[29] K.B. Ben Mahmoud, J. Thermophys. Heat Transfer 23 (2009) 409.
[30] T.G Zhao, Z.S. Wang, K.B. r Ben Mahmoud, Int. J. Math. Comput 1 (2008) 13.
[31] K. Boubaker, Trends Appl. Sci. Res. 2 (2007) 540.
[32] K. Boubaker, NMPDE 25 (2009) 802.
[33] S. Slama, J. Bessrour, B. Karem, M. Bouhafs, Proc. of COTUME'08 (2008) 79.
[34] H. Labiadh, M. Dada, O.B. Awojoyogbe, K.B. Ben Mahmoud, A. Bannour, J. Diff. Eq. Cont. Proc. 1 (2008) 51.
[35] O.B. Awojoyogbe, K. Boubaker, Curr. App. Phys. 9 (2009) 278.
[36] J. Ghanouchi, H. Labiadh, K. Boubaker, Int. J. Heat Technol. 26 (2008) 49.
[37] S. Slama, M. Bouhafs, K.B. Ben Mahmoud, Int. J. Heat Technol. 26 (2008) 141.
[38] K. Boubaker, Far-East J. Appl. Math. 31 (2008) 299.
[39] D.H. Zhang, F.W. Li, IJAP Lett. 2 (2009) 25.
[40] F. Xu, Z.Y. Yuan, G.H. Du, M. Halasa, B.L. Su, Appl. Phys. A 86 (2007) 181.
[41] Y.R. Park, E.K. Kim, D. Jung, T.S. Park, Y.S. Kim, Appl. Surf. Sci. 254 (2008) 2250.
[42] G. Machado, D.N. Guerra, D. Leinen, J.R. Ramos-Barrado, R.E. Marotti, E.A. Dalchiele, Thin Solid Films 490 (2005) 124.
[43] A. Sugiyama, J. Fluoresc. 16 (2006) 461.
[44] L. Xu, Y. Su, Y. Chen, H. Xiao, L. Zhu, Q. Zu, S. Li, J. Phys. Chem. B. 110 (2006) 6637.
[45] J. Jie, G. Wang, X. Han, Q. Yu, Y. Liao, G. Li, J. Hou, Chem. Phys. Lett. 387 (2004) 466.
[46] J. Liu, Y. Zhang, J. Qi, Y. Huang, X. Zhang, Q. Liao, Mater. Lett. 60 (2006) 2623.
[47] A. Ortíz, M. García, C. Falcony, Thin Solid Films 207 (1992) 175.
[48] R. Kun, M. Szekeres, I. Dékány, Appl. Catal. B 68 (2006) 49.
[49] G.Z. Xing, B. Yao, C.X. Cong, T. Yang, Y.P. Xie, B.H. Li, D.Z. Shen, J. Alloys Compd. 457 (2008) 36.

[50] B. Wang, M.J. Callahan, C. Xu, L.O. Bouthillette, N.C. Giles, D.F. Bliss, J. Cryst. Growth 304 (2007) 73.
[51] A. Tiburcio-Silver, J.C. Joubert, M. Labeau, J. Phys. III 2 (1992) 1287.
[52] E. Pál, I. Dékány, Colloids Surf. A: Physicochem. Eng. Aspects 318 (2008) 141.
[53] M.N. Jung, E.S. Lee, T.-I. Jeon, K.S. Gil, J.J. Kim, Y. Murakami, S.H. Lee, S.H. Park, H.J. Lee, T. Yao, H. Makino, J.H. Chang, J. Alloys Compd. 481 (2009) 649–653.
[54] C.E. Benouis, M. Benhaliliba, A. Sanchez Juarez, M.S. Aida, F. Chami, F. Yakuphanoglu, J. Alloys Compd. 490 (2010) 62–67.
[55] Y. Tao, M. Fu, A. Zhao, D. He, Y. Wang, J. Alloys Compd. 489 (2010) 99–102.
[56] M.R. Barati, J. Alloys Compd. 478 (2009) 375–380.
[57] T. Ratana, P. Amornpitoksuk, T. Ratana, S. Suwanboon, J. Alloys Compd. 470 (2009) 408–412.